Measurements of Lead Vapor and Particulate in Flames and Post-flame Gases

STEVEN G. BUCKLEY*
Department of Mechanical Engineering, University of Maryland, College Park, MD 20742, USA

ROBERT F. SAWYER
Department of Mechanical Engineering, U.C. Berkeley, Berkeley, CA 94720, USA

CATHERINE P. KOSHLAND
School of Public Health, Division of Environmental Health Science, U.C. Berkeley, Berkeley, CA 94720, USA

and

DONALD LUCAS
Advanced Energy Technologies Division, Lawrence Berkeley National Laboratory, Berkeley, CA 94720, USA

We describe several laser fluorescence methods used to measure lead in flames and in post-flame gases. Each relies on excitation of the 7s $^3P_1 \leftarrow 6p^2\ ^3P_0$ transition from the ground state of lead and detection of fluorescence on the 7s $^3P_1 \rightarrow 6p^2\ ^3P_1$ and 7s $^3P_1 \rightarrow 6p^2\ ^3P_2$ transitions. Aqueous solutions of lead salts are atomized and injected into a lean flatflame. Dye laser excitation is used to detect the formation of Pb atoms at the flame front, and to obtain a concentration profile in the post flame gases. Excimer laser fragmentation-fluorescence spectroscopy (ELFFS) is used to detect molecular gas-phase and aerosol compounds in the post-flame gases. A single-shot detection limit of 220 ppb for Pb species for the single-laser ELFFS technique has been determined in post-flame gases; the sensitivity of the technique is not seriously affected by the Pb species injected into the flame. A sharp rise in ELFFS Pb signal in the 600 to 750 K region from molecular and aerosol forms of Pb is attributed to homogenous nucleation of PbO. Two-laser fragmentation-fluorescence measurements with a variable delay time between photofragmentation and Pb atom detection indicate that chemical reactions may be an important removal step for Pb at elevated temperatures.

INTRODUCTION

Lead is a common component of municipal [1] and medical waste [2], and it is present in substantial quantities in coal, up to a few hundred parts-per-million (ppm) depending on the coal [3]. With the elimination of leaded gasoline throughout most of the United States, emissions from high-temperature processes such as coal combustion and waste incineration form the major sources of lead in the atmosphere in many parts of the U.S. The widespread use of lead in batteries contributes heavily to its presence in incinerable waste; an EPA study estimated that a typical concentration of lead in urban refuse is 230 ppm [4]. While Federal and California regulations limiting averaged (3-month) concentrations of lead to 1.5 $\mu g/m^3$ in ambient air are generally met [5], point sources which can cause locally unhealthy conditions are still a cause for concern [6].

In combustion systems, lead and other trace metals generally volatilize in the flame zone, react, and then (with the exception of mercury) become supersaturated in the cooling gas stream, condense and nucleate to form a metal aerosol [7, 8]. The net result of the nucleation and condensation processes is that submicron particles in the exhaust of a combustion device are often enriched in trace, toxic metal species [9, 10]. The submicron aerosol mode is respirable and itself is implicated in damaging health effects [11], which may be complicated by the presence of toxic metals such as lead.

Interest in the partitioning and fate of toxic metals in combustion systems has increased recently. The first comprehensive review of the subject specifically treating incineration processes was published by Linak and Wendt in 1993 [12]. Previous papers investigating the

*Corresponding author. E-mail: buckley@eng.umd.edu

COMBUSTION AND FLAME 128:435–446 (2002)

Published by Elsevier Science Inc.
0010-2180/02/$–see front matter
PII 0010-2180(01)00366-2

transformations of metals in combustion systems include the work of Mulholland and Sarofim [13], who injected a monodisperse, single component droplet spray of nickel, cadmium, and lead into an isothermal downflow reactor and investigated the resulting particle size distribution as a function of temperature. Similar work with the addition of chlorine to the system has been continued by Linak and co-workers [14]. Other researchers have investigated the aerosol dynamics evolving from lead in flames [15–18].

While most researchers have focused on the formation of aerosols and metal emissions in the exhaust of combustion systems, few have examined the high-temperature region around flames containing toxic metals, and as a result there is a dearth of knowledge about the flame structure and chemical kinetics of most metals in high-temperature environments. Recent work investigating the structure of a low-pressure propane flame doped with ~100 ppb manganese additive [19], and the work of Kennedy and co-workers on arsenic and chromium-doped flames [20, 21] are exceptions. Ehrman and coworkers have recently studied transformation of binary ZnO/MnO and CuO/MgO particles in a flame [22]. They observed large, unagglomerated particles that persisted through the flame, and small agglomerates probably formed via homogeneous nucleation. The results in their low-temperature ($\Phi = 0.66$) flame suggested that vaporization and chemical reaction were important limitations in the formation of aerosol for these relatively refractory species. Recent PbO planar laser-induced fluorescence (PLIF) measurements by Biswas and Zachariah with silica sorbants in Pb-doped flames and high-temperature furnace reactors illustrated the effect of sorbants and suggested that there were no kinetic or mass-transfer limitations in the incorporation of gas-phase PbO into a silica sorbant [23]. The PLIF measurements were able to reveal the streamwise reduction in gas-phase PbO.

In general, little can currently be predicted about metals chemistry; thermodynamics only recently have been applied to many high temperature toxic metal systems [24]. The study of Cosic and Fontijn [25] of the kinetics of ground-state Pb reactions with N_2O, Cl_2, and HCl suggests that bimolecular reactions with these species may be reasonably fast in the 500 to 1,300 K temperature range, and that reactions with O_2 are very slow and dependent upon heterogeneous (i.e., surface) processes. As the available surface area is strongly dependent upon the particular combustion system under study, the last finding may indicate that chemical kinetics will not be suitable for determination of Pb reaction rates in the absence of detailed knowledge of the particle size distribution. Knowledge of higher temperature (i.e., Pb + O = > PbO, Pb + OH = > PbO + H) kinetics that may be important at flame temperatures is also lacking. For these reasons, the ability to make measurements of Pb in high-temperature reacting flows is important.

The goal of this work is to present the use of excimer laser fragmentation-fluorescence methods for measurements of metal species in flames, using Pb as an example system. In this work we show that these methods are able to track the formation of Pb atoms at the flame front, their reaction to form molecular species, and subsequent nucleation of particles in the cooling post-combustion gases. The characteristics of the diagnostic method are explored alongside the characteristics of the Pb combustion system.

LASER DIAGNOSTIC METHODS

In this paper we use excimer laser fragmentation-fluorescence (ELFFS) spectroscopy for detecting toxic metal species. In ELFFS, an excimer laser is used to photofragment molecules. Excess energy from photofragmentation can excite electronic states of fragment atoms and molecules, which are detected using fluorescence. A 193 nm ArF excimer laser is close enough to the vacuum UV that most molecules have a significant absorbance of the laser light [26]; using the *single-laser ELFFS* technique we detect six out of twelve toxic metals tested in post-flame gases, including Pb [27]. Other researchers have used this technique to measure concentrations of alkali metals in coal combustors [28–30]. The relevant energy levels of Pb are shown in Fig. 1. When single-laser ELFFS is conducted in post-flame gases containing Pb, all

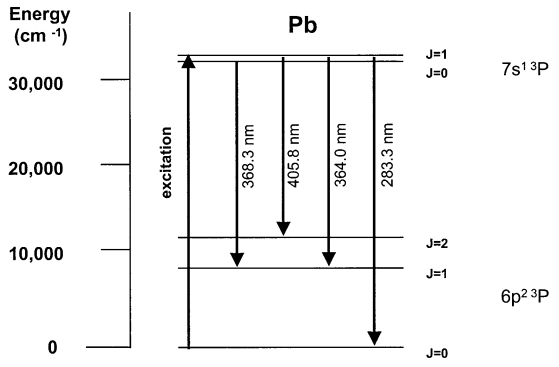

Fig. 1. Relevant energy levels of Pb.

of the emission lines in Fig. 1 are observed. Single-laser ELFFS excites fluorescence from molecules and from particles containing metals.

A variant of ELFFS is the *two-laser ELFFS* technique, which we have used previously to measure chlorinated hydrocarbons [31, 32]. Here a second laser probes the fragment molecules to excite fluorescence. In the case of Pb, we excite ground state atomic fluorescence; hence this measurement yields emission from both nascent Pb(g), and Pb(g) produced from photofragmentation of either aerosol or molecular species. Two-laser ELFFS allows probing of the decay of Pb(g) following photofragmentation, which may be as a result of reaction or condensation. The same emission lines are observed as in the LIF measurements.

We also employ conventional laser-induced fluorescence (LIF) techniques to detect Pb atoms as well as other species. When UV light from the dye laser at 283.3 nm excites the $7s^1\ ^3P_1 \leftarrow 6p^2\ ^3P_0$ transition, fluorescence is observed from the upper state to the three lower states shown in the figure.

The measurements described here are taken in atmospheric pressure flames and post-flame gases, where significant temperature gradients and quenching variations occur. No corrections have been applied to the observed fluorescence signals, hence these measurements are qualitative.

EXPERIMENT

A schematic of a typical experiment is shown in Fig. 2. Methane-air flames supported on a 3-cm diameter Meeker burner are used for most of the experiments. The burner supports flames with an equivalence ratio (Φ) as low as 0.6; the $\Phi = 0.8$ flatflame used for the majority of the work has a total (cold-gas) flowrate of 61 cm^3/s. The burner is shrouded by a 3.25 cm inner diameter copper tube to prevent entrainment of room air into the post-flame gases. Flows are metered using rotometers, combined in a gas manifold, and arrive at the burner premixed.

Metals are introduced using a TSI model 9032 nebulizer that atomizes a prepared solution of a lead salt. Metal salts used are at least 98% purity, obtained from Aldrich. The bulk flow of the atomizer was calibrated using two methods: capture of aerosol in an impinger train followed by both UV absorption measurements of the resulting ion concentration using a

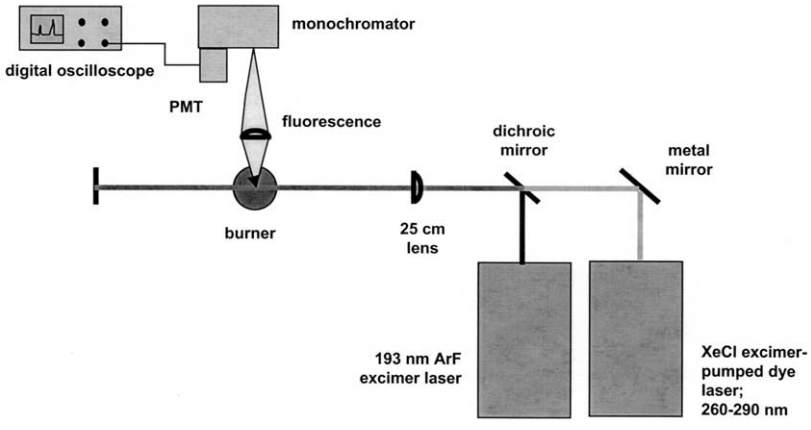

Fig. 2. Experimental setup.

Hewlett Packard 8452A absorption spectrometer, and by the Mohr method for determination of chloride in solution [33]. The concentration is varied in the flame by changing the concentration of the metal salt solution. The flow from the atomizer was combined with the premixed gas stream 15 cm upstream of the burner surface. Unless noted otherwise in the text, $Pb(NO_3)_2$ was added to the flame at 2 ppm.

The Lambda Physik EMG 102 MSC ArF excimer laser used for photofragmentation develops 120 mJ pulses of 193 nm light, which are focused into the detection region using a 25 cm focal length UV grade plano-convex fused silica lens. This creates a minimum laser cross-section of 2×0.5 mm with a peak intensity of 1.2×10^5 J/m^2, which given the 20 ns pulse width of the laser is roughly an order of magnitude less than the peak power which would be needed for optical breakdown in a typical combustion device [34]. Because the photofragmentation laser is only mildly focused, and the creation of a plasma is avoided, thermal effects are negligible. Calculations based on measured laser absorption show that the maximum temperature rise in the detection region is less than 100 K.

A Lambda Physik FL 3002 excimer-pumped dye laser generates tunable laser light. A barium borate (BBO) crystal doubles the fundamental light from the Coumarin 153 dye solution to yield a tunable range of 260 to 290 nm. The pulse energy at the lead excitation wavelength of 283.3 nm is 11 μJ. For the majority of the experiments, this light was combined colinearly with the excimer light and focused using the same 25 cm lens, as shown in Fig. 2. The dye laser beam is roughly 1.5×0.3 mm in cross section at the focus; the long axis of the beam is perpendicular to the long axis of the excimer, making the overlap region 0.5×0.3 mm.

The laser light is focused above the center of the burner. Translation stages allow controlled burner movement and positioning in three orthogonal directions. Fluorescence from the detection region is collected at right angles and imaged using a single 5-cm focal length plano-convex lens onto the entrance slit of a 0.3 m McPherson scanning monochromator. The 0.4-mm monochromator slitwidth corresponds to a bandpass of 1.1 nm. A 280-nm cut-on high-pass Schott glass filter (WG-280, CVI Laser Corp.), mounted at the entrance to the monochromator, rejects scattered 193 nm light from the photofragmentation laser. The light passing through the monochromator enters a Hammamatsu R928 photomultiplier tube (PMT); the generated signal is digitized using a LeCroy 9410 digital oscilloscope and sent to a PC for storage and processing. For fluorescence spectra, the maximum signal from the PMT is recorded as the wavelength is varied. Typically data from fluorescence scans are averaged over 5 shots to reduce the noise; this is less than 20% of the bandpass of the monochromator at the normal scan resolution of 24 shots/nm.

Additional experimental information can be found in the literature [27, 35].

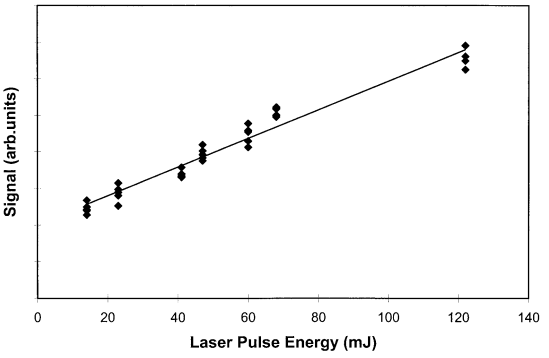

Fig. 3. Single-laser photofragmentation signal dependence of Pb 405.8 nm line on excimer pulse energy. Each point is the average of 100 laser shots.

RESULTS AND DISCUSSION

Characteristics of the LIF and ELFFS Measurements

Single-laser ELFFS measurements taken in post-flame gases are linear with both incident laser power and concentration for low concentrations of Pb. As an example, Fig. 3 shows the ELFFS signal as a function of incident laser power, which was varied using a succession of screens of various mesh sizes placed in the beam path to affect partial absorption of the laser beam. Power was measured using a Gentech laser power meter. Pb was injected into the $\Phi = 0.8$ flat flame at a concentration of 1 ppm, and the measurements were made in post-flame gases at a point 5 cm above the flame. Each

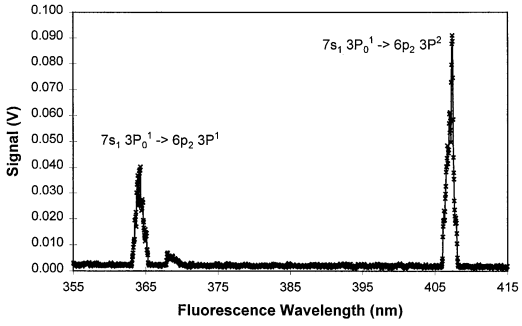

Fig. 4. Fluorescence scan from injection of 2 ppm of lead nitrate into $\Phi = 0.8$ flatflame with dye laser tuned to 283.3 nm Pb transition, taken 0.3 cm above flatflame.

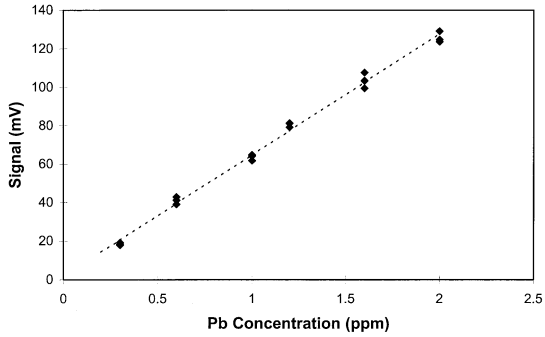

Fig. 5. Dependence of laser-induced fluorescence of Pb on concentration.

point shown is a 1000-shot averaged signal recorded at 5 Hz, and the line drawn through the data points is a least-squares fit of the data. Similar to Fig. 3, the response of the ELFFS signal to changing concentration under similar conditions is also linear. When the dye laser is tuned to the $7s^1\ 3P^o_1 \leftarrow 6p^2\ 3P_0$ Pb transition at 283.3 nm in post-flame gases seeded with Pb, two prominent Pb peaks at 364.0 and 405.8 nm are observed, corresponding to the $7s^1\ 3P^o_1 \rightarrow 6p^2\ 3P_1$ and $7s^1\ 3P^o_1 \rightarrow 6p^2\ 3P_2$ transitions illustrated in Fig. 1 [36]. Fig. 4 shows a fluorescence scan taken over the 355 to 415 nm wavelength region in the post-flame region 0.5 cm above the $\Phi = 0.8$ flatflame with 2 ppm of Pb injected as lead nitrate solution.

The background signal observed when the dye laser is tuned off the Pb transition is less than 1 mV, mostly attributable to EMF noise generated by the firing of the 308 nm XeCl excimer laser used to pump the dye laser. The RMS background signal observed when the laser is tuned off the Pb excitation is roughly 280 times smaller than the peak signal corresponding to the injection of 2 ppm of Pb into a $\Phi = 0.8$ flat flame. When the laser is tuned on to the Pb transition, the RMS deviation in the fluorescence scan background for the same flame is ~220 times smaller than the peak. These measurements of the ratio of the peak intensity to the average noise would suggest a detection limit (defined as three times the RMS level) of ~30 ppb, using the conservative estimate that Peak/RMS = 200 for the 2 ppm flame, and assuming complete atomization in the flame.

Figure 5 shows 2-laser ELFFS signal response, laser-induced fluorescence signal following photofragmentation of different concentrations of Pb. The flame concentration was varied over the range 0.2 to 2 ppm, and 3 data points averaging 500 laser shots at 10 Hz were taken at each concentration. These measurements were obtained in the high-temperature region ~0.3 cm above the $\Phi = 0.8$ flat flame with a delay time of 0.35 μs (long enough such that fluorescence because of photofragmentation has completely decayed) between the fragmentation laser and the dye laser. The flame location was determined visually. At this proximity to the flame, which has an adiabatic flame temperature of 2,000 K, no thermocouple temperature measurements were attempted because of the potential for inaccuracy as a result of radiation and conduction effects. Pb was excited at 283.3 nm and fluorescence observed at 405.8 nm. The line drawn through the data are a linear regression of the data. Over the range of concentrations tested, these LIF measurements exhibited a linear response to concentration, indicating that neither self-absorption or significant absorption of the laser is an issue at these concentrations.

Various lead salts (chloride, acetate, bromide, and nitrate) injected into the flame at 2 ppm concentration all exhibit nearly identical response when single-laser ELFFS measurements are taken at ~800 K in the post-flame region. This indicates that the flame acts as an equally effective atomizing agent for each of these salts.

Figure 6 shows a single-shot, single-laser ELFFS spectra taken for 2 ppm $Pb(NO_3)_2$

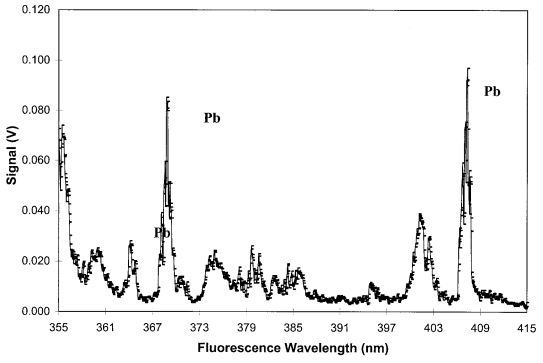

Fig. 6. Single-laser ELFFS fluorescence scan in the post-flame region.

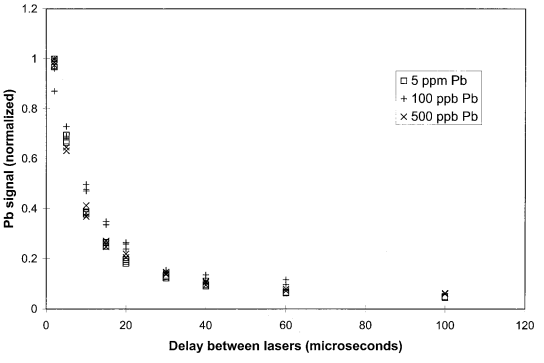

Fig. 7. Variation in 2-laser ELFFS Pb fluorescence as a function of delay time for various Pb concentrations.

injection in this cooler post-flame region. Comparing this spectrum to the dye laser fluorescence spectrum in Fig. 4, the 368.3 nm line originating from the $7s^1\ ^3P_0$ state is much more prominent, while the 364 nm fluorescence is much weaker. This difference is attributable to the fact that the photodissociative excitation can excite either of the two levels of the excited state, while the dye laser only excites J = 1. In addition, background signal from post-flame gas species excited and ionized by the excimer laser, including O_2, CO^+, CO_2^+, and other species can be identified. As above, the single-shot limit of detection is calculated to be ~30 ppb using this technique, based on a measured signal-to-noise ratio (SNR) = Peak/RMS of $(1.13 \times 10^{-1})/(5.54 \times 10^{-4}) = 204$ on the 405.8 nm line.

In the present configuration the 2-laser ELFFS technique, in which ground state atomic concentration is measured following photofragmentation, is more sensitive than the single-laser ELFFS technique in the region of burned gases more than 2.5 cm above the burner, where the temperature is less than 500 K. The measurements in Fig. 5 were obtained with a delay between the two laser pulses of 0.35 μs. The 2-laser ELLFS signal is a strong function of the delay between the photofragmentation laser and the dye laser; the decay in Pb signal under the conditions of the flame is ~90% in 40 μs. To investigate this further, studies were conducted using a flow reactor. The hypothesis was that the 193 nm light produces lead atoms from compounds or particles, and the decay observed as the delay time between the two lasers increased was either because of nucleation or chemical reaction. To determine whether or not the disappearance of Pb was as a result of nucleation, the concentration of Pb was varied over the widest possible range to affect the nucleation characteristics. To determine if reactions with oxygen were important, the equivalence ratio of the flame was varied while the concentration of Pb was kept constant.

Figure 7 illustrates the effect of changing Pb injection concentration on the two-laser ELFFS signal. Lead acetate was injected into the flow reactor at concentrations corresponding to 100 ppb, 500 ppb, and 5 ppm of Pb in the flame. The flame was at an equivalence ratio of 0.71, and the temperature at the measurement point was 600 K. Considering the Pb atoms that are formed from photofragmentation, Pb would be supersaturated for any of the concentrations tested [37]. However, because Pb nucleation is very sensitive to the degree of supersaturation, it was expected that some change might be seen in the signal as a function of delay, as concentration was strongly varied between 100 ppb and 5 ppm, if nucleation were the dominant removal mechanism for Pb atoms formed by the fragmentation laser. However, the data in Fig. 7 show an identical decay curve for all concentrations of Pb injected into the flow reactor, consistent with a reaction that is first order in [Pb], and is faster than nucleation, where characteristic times are on the order of milliseconds [38].

Changing the equivalence ratio had a dramatic effect on the two-laser ELFFS signal as a function of delay time, as shown in Fig. 8. Lead acetate was injected into the flow reactor at a flame concentration of 500 ppb, and the equiv-

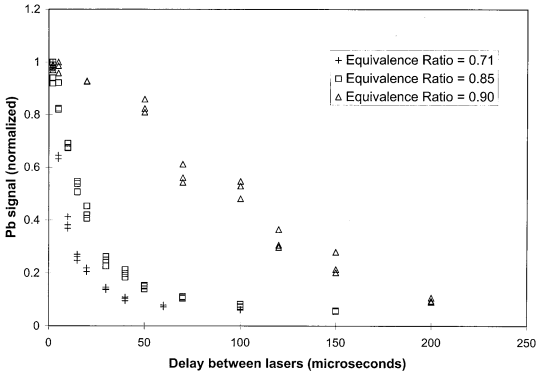

Fig. 8. Variation in 2-laser ELFFS Pb fluorescence as a function of delay time for various equivalence ratios.

alence ratio was adjusted to 0.71, 0.85, and 0.90 in subsequent measurements. The measurement temperature was kept constant at 600 K by adjusting the movable flameholder. Each data point is a 100-shot average taken at 10 Hz; three data points were taken for each condition. As seen in the figure, decreasing the equivalence ratio increases the decay rate of Pb following the photofragmentation laser shot.

A major effect of decreasing the equivalence ratio is to increase the mole fraction of O_2 in the burned gases. Kinetic data from Husain and Littler [39, 40] were used to estimate the rate of Pb + O_2 + M $\Rightarrow$ products. In this work, flash photolysis of tetraethyl lead at temperatures up to 573 K had yielded a termolecular Arrhenius pre-exponential A = 1×10^{-31} $cm^6/(mol^2 * sec)$ and an activation energy E = −9.62 kJ/mol. A third body concentration of 1×10^{19} molecules/cm^3 yields a reaction rate constant

$$k = (1 \times 10^{-12}) \exp\left(\frac{9.62kJ}{RT}\right) \frac{cm^3}{mol \cdot s}.$$

With these parameters, the predicted time for the reaction to go to 90% completion at $\Phi = 0.8$ with 2 ppm of Pb is 1.2 ms. Hence, the reaction of Pb with O_2 is too slow by more than an order of magnitude to predict the measured decay following the fragmentation pulse. This is consistent with more recent measurements of the Pb + O_2 rate [25], which indicate that the homogeneous rate is very slow, and that heterogeneous reactions dominate the reactions of Pb with diatomic oxygen. Hence the reduction in Pb signal as the delay between the fragmentation and the probe lasers increases is caused by heterogeneous reactions of Pb + O or Pb + O_2 on surfaces. As will be further substantiated below, this is consistent with the nucleation of PbO or PbO_2 in the post-flame region. PbO is the expected product at higher temperatures, based on both measurements [23] and equilibrium calculations [24], and nucleation would form a large number of small particles with a large surface area, which would facilitate heterogeneous reactions.

Another reaction mechanism that could explain the decay of Pb is the photolysis of O_2. Excited O_2 in the predissociative $B^3\Sigma_u^-$ state (the Schumann-Runge bands) is formed by 193 nm light [41], producing two $O(^3P)$ atoms [26]. The reaction $O_2 + O(^3P) \Rightarrow O_3$ has a quantum yield of 0.3 at atmospheric pressure [42]. Reaction of Pb with $O(^3P)$ or O_3 would likely be faster than Pb + O_2, resulting in the increased rate of Pb decay with increasing O_2 concentration. Other oxidation reactions, including Pb + OH + M or Pb + N_2O may also be important in the removal of atomic Pb, but little is known about these kinetics. The formation of a lead oxide is consistent with equilibrium calculations, which predict the formation of an oxide over atomic Pb or Pb_2 in a lead-oxygen system at any temperature between 200 and 1,600 K, but calculations by Wu and Biswas omitted PbOH as a possible product, presumably because of insufficient thermodynamic data [24]. Chertihin and Andrews [43] identified the matrix-isolated products of laser ablated lead in oxygen/argon and oxygen/nitrogen environments, including PbO, OPbO, $Pb(O)_2$, $PbPb(O)_2$, Pb_4O_4, and ozone. The lead monoxide and linear lead dioxide were not observed with thermally produced lead atoms, indicating that several species may be involved in the reactions we observe.

In-Flame and Atomic Concentration Measurements

When a Pb-containing aerosol is added to a flame, lead atom signals are generated at the flame front and persist in the post-flame gases. Figure 9 illustrates the production of Pb atoms in a rich $\Phi = 3$ flame, where the flame is lifted off the burner and looks like a completely non-premixed flame. The LIF measurements of

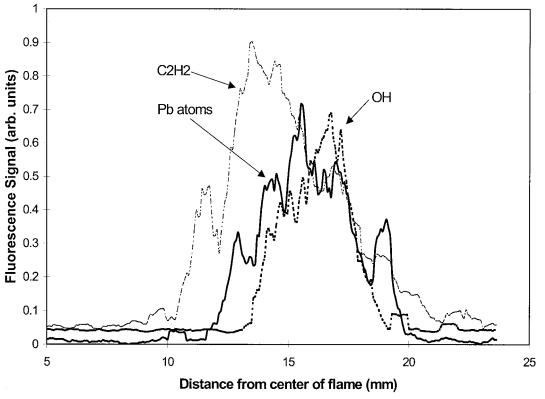

Fig. 9. Production of Pb atoms at the flame front of a partially premixed ($\Phi = 3$) flatflame.

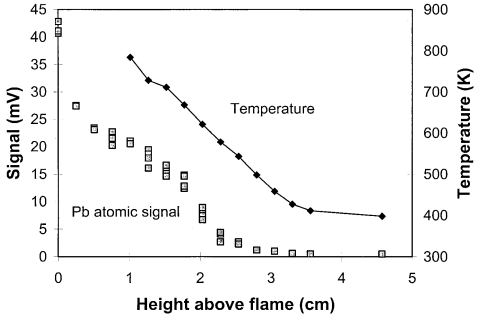

Fig. 10. Atomic Pb signal from dye laser excitation above flat flame as a function of height above the burner.

Pb atoms were taken using the dye laser alone. The dye laser scans from the center of the unburned gases radially outward through the flame front using a stepper-motor controlled translation stage that scans at a precisely controlled rate. The *x*-axis of the figure is distance from the centerline of the burner. This scan was taken close to the burner surface, where fluctuations affect the flame location the least. The three peaks shown in Fig. 9 correspond to C_2H_2, Pb, and OH. C_2H_2 is observed using 193-nm photofragmentation followed by detection of emission on the CH $A^2\Delta \rightarrow X^2\Pi$ transition at 317 nm as described by Allen and Hanson [44]. Pb is detected using the 405.8 emission line, as above. The OH radical is excited on the (1–0) Q branch of the $A^2\Sigma \leftarrow X^2\Pi$ transition at 282.9 nm, and emission from the (1–1) band is monitored at 312.5 nm with a monochromator bandpass of 2.5 nm to catch fluorescence from both the R_1 and R_2 bandheads. The data illustrates that the production of Pb atoms begins to rise between the C_2H_2 and OH peaks. After scanning through the flame the laser moves into room air, and the Pb signal falls off quickly. The maximum value of the Pb signal is ~240 times greater than the RMS signal in the region of x = 5 to x = 8 mm, where no Pb fluorescence is expected.

Dye laser fluorescence measurements shown in Fig. 10 illustrate that the Pb fluorescence signal can be detected up to 2.5 cm above the burner in the post-flame gases of the flat flame. The burner is physically shrouded to minimize mixing of room air. Each point is the average signal from 200 shots of the laser. The signal falls off somewhat immediately following the flame, and then again as the gases cool from 750 to 600 K. The atomic fluorescence signal measured at 900 K is linear with the concentration of injected Pb, and can be measured down to the lowest injected concentration of 200 ppb with a signal-to-noise ratio of 6.

The measurements in Figs. 9 and 10 together illustrate the conversion of Pb from the lead salts in the fuel stream to Pb(g), and further illustrate the reaction of Pb(g) in the post-flame zone to form molecular species. Used in the appropriate flame configuration (e.g., a counterflow flame) measurements with ELFFS could thus be used to extract much-needed kinetic data for metal species at high temperatures.

Aerosol and Post-flame Measurements

Following the flame, Pb(g), PbO, and other Pb-containing products are expected to form aerosol particles, which evolve downstream of the flame. ELFFS was used to probe the region downstream of the flame to observe the response of the diagnostic to the changing conditions. Signals from the single-laser ELFFS and 2-laser ELFFS detection schemes above the flame are shown in Fig. 11. The single-laser ELFFS scheme measures Pb fluorescence of excited products from fragmentation of PbO, PbO_2, and aerosol, while the 2-laser scheme excites Pb fluorescence from ground state products. The signals rise slowly downstream of the flame, peak in the 750 to 600 K temperature region, and then fall to a relatively constant value in the cooler regions below 450 K. The

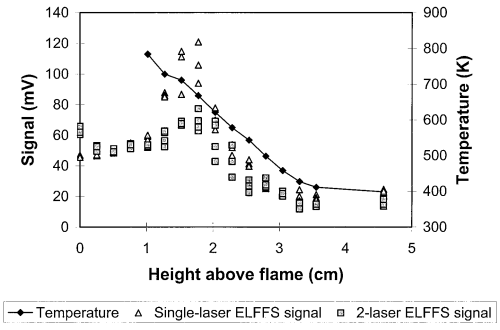

Fig. 11. Single and 2-laser ELFFS signals as a function of height above burner.

single-laser and 2-laser ELFFS signals exhibit similar responses.

The data in Fig. 11 can be compared with similar single-laser ELFFS data taken in a flow reactor, shown in Fig. 12. In this case a $\Phi = 0.87$ methane/air flame with 3 ppm lead acetate was stabilized in a 1-meter, 3.25 cm-diameter flow reactor with a movable flameholder. The moving flameholder was used to adjust the temperature at the exit of the reactor where Pb fluorescence was measured. The temperature dependence of the post-flame signal shows a similar trend, in this case peaking at about 770 K.

From equilibrium, PbO and Pb are expected to be the principal lead species from these flames [14, 15], possibly formed because of the reaction $Pb + N_2O => PbO + N_2$ (which is much faster then the gas-phase $Pb + O_2$ reaction) [25] or heterogeneous wall or particle reactions. PbO and Pb have vapor pressures corresponding to a concentration of 2 ppm at 956 K and 945 K [37]. As the gas stream cools

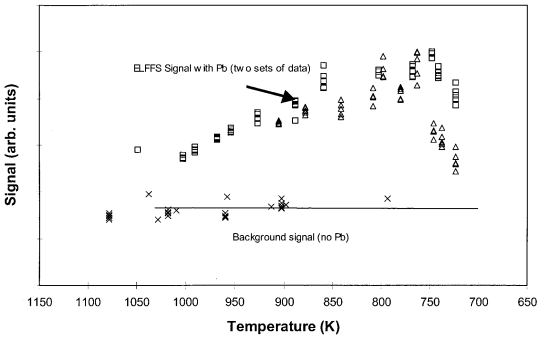

Fig. 12. Single-laser ELFFS in post-flame of 0.87 flow reactor with 3 ppm Pb injection.

and these lead species become supersaturated, condensation and nucleation will occur [45]. The increased signal observed in both Figs. 11 and 12 in the 600 to 800 K temperature region is believed to be because of the sudden onset of nucleation, expected under these conditions [46]. An increase in photofragmentation-fluorescence signal is typically observed from particles, as the photofragmentation laser may ablate some or all of a particle, forming excited fragments that subsequently fluoresce.

Homogenous nucleation of vapor phase species can occur when the cooling rate of gases is sufficiently rapid that condensation alone cannot keep the degree of supersaturation below a critical value. The onset of nucleation has been studied in similar systems of zinc and magnesium oxides, where it generates a high concentration of particles in the 10 to 40 nm size range, which subsequently coagulate to form larger particles [17]. Measurements in a bench scale swirl flame incinerator with $\Phi = 0.83$ and 100 ppm $Pb(NO_3)_2$ injection found that the mean diameter of the final aerosol was ~200 nm [14]. Rapid production of aerosol could be causing the observed increase in signal; this hypothesis is supported by the observation that the peak in signal occurs at a slightly higher temperature in the flow reactor than the flatflame. The higher concentration of Pb in the flow reactor should cause earlier inception of nucleation.

To confirm the hypothesis that aerosol particles are responsible for the increased signal, metal aerosol is generated using the atomizer in non-flame experiments. Unfortunately, PbO aerosol can not be investigated because of its very low solubility in water, but several other soluble lead salts are used. The output of the atomizer is combined with the same flow of air used in the flame experiments. From calculated droplet evaporation rates [47] the aerosol is expected to be dry following mixing with the carrier air. The majority of the aerosol produced following evaporation of the water should correspond to a single particle per droplet [14]. These particles are calculated to have a mean diameter of 72 nm when the solution concentration is 0.01 M. Comparison of the signal generated at 405.8 nm from $PbCl_2$ aerosol following excitation by the 2-laser ELFFS technique and by the dye laser alone reveals no

TABLE 1

Comparison of the response of single-laser ELFFS to room-temperature aerosol compared with postflame gases at 450 K.

Aerosol species	Ratio aerosol/postflame
Lead acetate	43
Lead nitrate	45
Lead bromide	66
Lead chloride	62

response from the dye laser alone, but a strong atomic signal following the excimer pulse. Other experiments demonstrate that aerosols exhibit a similar strong response from single-laser ELFFS. The single-laser ELFFS signal generated from 72 nm aerosol has been measured for several different Pb solutions, as shown in Table 1. The tested aerosols generated a response between 43 and 66 times greater than the signal corresponding to the same concentration in the post-flame gases at 450 K.

The ELFFS signal generated by different sizes of particles has been observed to vary with the total surface area of the particles. Changing the solution concentration of the metal salt should change the mean diameter of the particles that are produced by the nebulizer, but not the number concentration of the particles. Figure 13a shows the Pb signal generated from aerosol as a function of mean calculated particle size, while Fig. 13b shows the same data, dividing the signal by the relative total surface area of the particles in the plume. The results suggest that the ELFFS signal has a strong dependence on the aggregate surface area of particles in the plume, consistent with a surface ablation effect for these particles, rather than complete vaporization. This result could explain the decline in ELFFS signal observed in Figs. 11 and 12 as the gases cool; as the particle size distribution matures in the cooling gas stream, the concentration of Pb species stays the same but the surface-to-volume ratio for the larger aerosol is smaller. Further work on the size and surface area dependence of the ELFFS signal from aerosol is warranted when direct measurement of the aerosol size can be accomplished. Other metals tested exhibit a much lower aerosol sensitivity (e.g., 124 nm $MnCl_2$ aerosol only generates 2.5 times greater signal than post-flame gases), and the sudden rise in signal that we attribute to nucleation of Pb species is not observed.

The post-flame measurements in Figs. 11 and 12 illustrate that ELFFS can be used to observe formation of Pb-containing particles in high-temperature systems. Further, the data in Fig. 13 suggest that ELFFS has a signal response that is linear with respect to the particle surface area, which indicates a surface ablation effect. Further work on this dependence is needed to both confirm the measurements and to determine whether different types of particles exhibit varying signal characteristics, for example as a function of their composition or morphology.

CONCLUSIONS

We have used LIF, single-laser ELFFS, and 2-laser ELFFS to measure Pb and Pb-containing species. The use and characteristics of each of these measurement tools has been illustrated, and the evolution of Pb and Pb-containing species in the flame has been presented. Pb was observed to be produced at the flame front, and to largely oxidize in the high-temperature regions ($T > 1{,}000$ K) of the post-flame zone. Nucleation of Pb-containing species presumed to be PbO is observed at temperatures in the 600 to 800 K range, consistent with injected concentrations. Both the ELFFS and 2-laser ELFFS techniques are shown to have a linear response to injected Pb concentration, and the ELFFS technique is shown to have a linear response to the pulse energy of the photofragmentation laser. The estimated detection limit for the 2-laser ELFFS technique is 30 ppb, while the single-shot estimated detection limit of the single-laser ELFFS technique is ~220 ppb. We show that oxidation reactions following the photofragmentation pulse affect the Pb fluorescence in the 2-laser ELFFS measurement, probably as a result of the reaction of atomic lead with either $O(^3P)$ or with O_3.

In the post-flame gases both single-laser ELFFS and 2-laser ELFFS are used to detect Pb species. Both signals show a sharp maximum in the temperature region from 600 to 750 K, which from vapor pressures could be attributed to either homogenous nucleation of PbO or Pb.

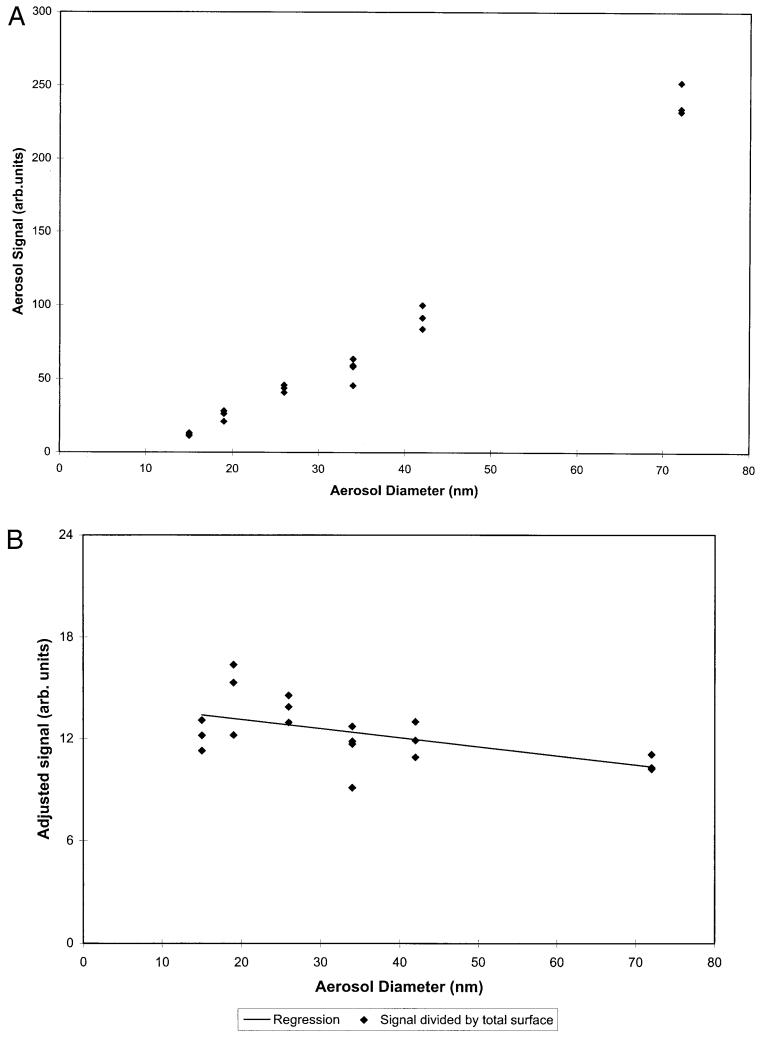

Fig. 13. (a) Single-laser ELFFS signal as a function of calculated aerosol diameter. (b) Single-laser ELFFS signal normalized by surface area as a function of calculated aerosol diameter.

Experiments show that ELFFS is much more sensitive to Pb aerosol than to gas-phase Pb species, and thus the sharp rise in signal is consistent with nucleation processes occurring at these temperatures. We postulate that the ELFFS signal response to aerosol is proportional to the total surface area of particulate, which suggests that the observed decrease in ELFFS signal as the gases cool below the 600 to 750 K temperature range is because of the decreasing total surface area of the particles as they agglomerate. Further work on this issue is warranted.

Additional work with these techniques is expected to yield significant new data about the kinetics of metals in flames and high-temperature processes that is vitally needed for understanding these processes and control of undesirable metal emissions from practical combustion processes.

This research was funded by contract P42ES04705 of the National Institute of Environmental Health Sciences Superfund Basic Research Program, as well as by the State of California Toxic Substances Research and Teaching Program. The authors would like to thank Chris Damm for insightful discussions and his continuing interest in this work.

REFERENCES

1. Kauppinen, E., Larjava, K., and Hillano, R., *J. Aerosol Sci.* 17:597–601 (1986).
2. Walker, B. L., and Cooper, C. D., *J. Air Waste Man. Assoc.* 42:784–791 (1992).
3. Smith, R. D., *Prog. Energ. Combust. Sci.* 6:53–119 (1980).
4. Edwards, L. O., et al., *Trace Metals and Stationary Conventional Combustion Processes*, 1981, U.S.E.P.A.
5. California Air Quality Data. *Summary: Gaseous and Particulate Pollutants*, California Air Resources Board, 1991.
6. McLaughlin, C., *Proposed Airborne Toxic Control Measure for Emissions of Toxic Metals from Non-Ferrous Metal Melting*, California Air Resources Board, 1992.
7. Seeker, W. R., *Proc. Combust. Inst.* 23:867–885 (1990).
8. Barton, R. G., Clark, W. D., and Seeker, W. R., *Comb. Sci. Tech.* 74:327–342 (1990).
9. Kauppinen, E. I., and Pakkanen, T. A., *Atmos. Env.* 24A:423–429 (1990).
10. Davison, R. L., et al., *Env. Sci. Tech.* 8:1107–1113 (1974).
11. Pope, C., Dockery, D., and Schwartz, J., *Inhal. Toxicol.* 7:1–18 (1995).
12. Linak, W. P., and Wendt, J. O. L., *Prog. Energy Comb. Sci.* 19:145–185 (1993).
13. Mulholland, J. A., and Sarofim, A. F., *Environ. Sci. Technol.* 25:268–274 (1991).
14. Linak, W. P., Srivastava, R. K., and Wendt, J. O. L., *Comb. Sci. Tech.* 101:7–27 (1994).
15. Lin, W. Y., Sethi, V., and Biswas, P., *Aerosol Sci. Tech.* 17:119–133 (1992).
16. Sethi, V., and Biswas, P., *J. Air Waste Man. Assoc.* 40:42–46 (1990).
17. Matsoukas, T., and Friedlander, S. K., *J. Colloid Int. Sci.* 146:495–506 (1991).
18. Wu, C.-Y., and Biswas, P., *Env. Eng. Sci.* 17:41–60 (2000).
19. Westblom, U., et al., *Comb. Flame* 99:261–268 (1994).
20. Zhang, Y., et al., *Proc. Combust. Inst.* 27:1777–1783 (1998).
21. Yu, S., et al., *Proc. Combust. Inst.* 27:1639–1645 (1998).
22. Ehrman, S. H., and Friedlander, S. K., *Aerosol Sci. Tech.* 30:259–272 (1999).
23. Biswas, P., and Zachariah, M., *Environ. Sci. Tech.* 31:2455–2463 (1997).
24. Wu, C. Y., and Biswas, P., *Combust. Flame* 93:31–40 (1993).
25. Cosic, B., and Fontjin, A., *J. Phys. Chem.* 104:5517–5524 (2000).
26. Okabe, H., *Photochemistry of Small Molecules*, Wiley, New York, 1978, p. 431.
27. Buckley, S. G., *Laser Detection of Toxic Metals in Combustion Systems* in *Mechanical Engineering*, University of California, Berkeley, 1995, p. 186.
28. Chadwick, B. L., Domazetis, G., and Morrison, R. J. S., *Anal. Chem.* 67:710–716 (1995).
29. Hartinger, K. T., et al., *Proc. Combust. Inst.* 25:193–199 (1994).
30. Rensberger Weiland, K. J., Wise, M. L., and Smith, G. P., *Appl. Optics.* 32:4066–4073 (1993).
31. McEnally, C. S., et al., *Appl. Optics.* 33:3977–3984 (1994).
32. McEnally, C. S., et al., *Proc. Combust. Inst.* 25:325 (1994).
33. Fischer, R. B., *Quantitative Chem. Analysis,* Philadelphia, W. B. Saunders, 1961, p. 501.
34. Eckbreth, A. C., in *Laser Diagnostics for Combustion Temperature and Species: Energy and Engineering Science Series* (A. K. Gupta and D. G. Lilley, Eds.), Cambridge, MA: Abacus, 1988, p. 414.
35. Buckley, S. G., et al., *Proc. Combust. Inst.* 26:2455–2462 (1996).
36. Corliss, C. H., and Bozman, W. R., *Experimental Transition Probabilities of Spectral Lines of Seventy Elements*, Washington, DC: National Bureau of Standards, 1962, p. 562.
37. Smithells, C. J., *Smithells Metals Reference Book,* 7th ed. (E. A. Brandes and G. B. Brook, Eds.), Oxford: Butterworth-Heinemann, 1992.
38. Barrett, J. C., and Clement, C. F., *J. Aerosol Sci.* 22:327–335 (1991).
39. Husain, D., and Littler, J. G. F., *J. Photochem.* 2:247–253 (1974).
40. Husain, D., and Littler, J. G. F., *Combust. Flame* 22:295–298 (1974).
41. Laufer, G., McKenzie, R. L., and Huo, W. M., *Opt. Let.* 13:99–101 (1988).
42. Washida, N., Mori, Y., and Tanaka, I., *J. Chem. Phys.* 54:1119 (1971).
43. Chertihin, G., and Andrews, L., *J. Chem. Phys.* 105: 2561–2574 (1996).
44. Allen, M. G, and Hanson, R. K., *Proc. Combust. Inst.* 21:1755–1762 (1986).
45. Friedlander, S. K., *Smoke, Dust, and Haze*, Wiley, New York, 1977.
46. McNallan, M. J., Yurek, G. J., and Elliott, J. F., *Combust. Flame* 42:45–60 (1981).
47. Bird, R. B., Stewart, W. E., and Lightfoot, E. N., *Transport Phenomena*, Wiley, New York, 1960.

Received 14 February 2001; revised 15 November 2001; accepted 25 November 2001